Comparison of Flow Measurement by 4D Flow Magnetic Resonance Imaging and by Particles Image Velocimetry on Phantom of Abdominal Aortic Aneurysm

Yufei Wang, D. Joannic, Juillion Patrick, A. Keromnes, Monnet Aurélien, A. Lalande, J.-F. Fontaine

SMGroup

SM Vascular Medicine

Research Article

Comparison of Flow Measurement by 4D Flow Magnetic Resonance Imaging and by Particles Image Velocimetry on Phantom of Abdominal Aortic Aneurysm

Yufei Wang[1], David Joannic[1,2], Patrick Juillion[1], Alan Kemrones[3], Aurélien Monnet[4], Alain Lalande[5] and Jean-François Fontaine[1,2]*

[1]*Le2i FRE2005, CNRS, Arts et Métiers, Univ. Bourgogne-Franche Comté, France*
[2]*IUT Dijon-Auxerre, France*
[3]*DRIVE, Univ. Bourgogne-Franche Comté, France*
[4]*Siemens Healthcare, France*
[5]*Faculty of Medicine, University of Bourgogne-Franche Comte, France*

Article Information

Received date: Nov 17, 2016
Accepted date: Dec 25, 2016
Published date: Dec 30, 2016

***Corresponding author**

Jean-François Fontaine, Laboratory of electronics, data processing and image, University of Burgundy, IUT Dijon-Auxerre, France, Email: jffont@iut-dijon.u-bourgogne.fr

Keywords Abdominal Aorta Aneurysm; Aorta phantom; Fluid velocity measurement; Metrology in medical Imaging; PIV; MRI

Abstract

Predicting the rupture of Aortic Aneurysms is a complex problem that interests, from several decades, many researchers. The works on this issue are very complex, involving both the study of mechanical behavior of the artery as the flow of blood. The Magnetic Resonance Imaging (MRI) technique allows to obtain anatomic information of the arteries, than the flow inside thereof. The goal of this study is an inter comparison between flow data from MRI and those obtained by Particle Image Velocimetry (PIV). An experimental device simulating hemodynamic circulation is used. Initially in order to validate the device, the flow in a cylindrical glass tube is measured by these two techniques and then compared to a theoretical model. Secondly, the flow in a phantom in silicone, with an axisymmetric aneurysm, is evaluated with 4D flow MRI sequences and the measurements are compared with those obtained by PIV with good agreement. The ability of the MRI technique to measure the flow thus makes an essential device for the study of cardiovascular disease.

Introduction

Cardiovascular diseases and, in particular, aortic aneurysm causes a large number of deaths, and preoperative diagnosis is often difficult to establish because the data are manifold and complex. The commonly used criteria for diagnosis aortic aneurysm are based on the observation of the artery diameter and its temporal evolution is sometimes insufficient. However, other criteria have been proposed. Raghavan and Vorp showed that the volume of the Abdominal Aortic Aneurysm (AAA), rather than its diameter, is a better predictor of rupture [1]. In addition, Achille et al. notes that residual stresses affect the stress distribution [2]. Truijers et al. [3] reported that hypertension plays an important role in the stress level on aortic wall, and Rodriguez et al. demonstrated the influence of the shape of the aneurysm, concluding that short aneurysms are more serious when they exhibit asymmetries [4]. Reeps et al. constructed models using computed tomography scans, reporting that AAA with thrombus increases vessel rigidity and reduces the maximum stress by 20% to 40% but has the negative effect of altering blood flow [5].

In fact, the pertinent physical characteristic to evaluate is the tensile strength of the arterial wall, which is made up of living tissue, has a complex geometry and undergoes internal changes that are highly dependent on blood flow. Many studies have been conducted in recent years to better understand the involved phenomena in AAA. For example, the properties of the aorta and its mechanical behaviour have been studied in terms of its mechanical properties (e.g., modulus of elasticity, yield strength, breaking strength) and the characteristics that portend thrombus. Avril et al. showed that the behaviour of these tissues is anisotropic and depends heavily on the constituents of the aorta [6-11].

Other work has been carried out using numerical modelling of AAA to calculate stress in the arterial wall in conditions as close as possible to the true pathophysiologic conditions. In this sense, Tougara et al. [12] used a simple model of cylindrical aneurysm, and Scotti and Finol rebuilt the shape of the aorta from CT images to generate a realistic anatomy [13]. In addition, Wang et al. reconstructed and studied a sacculi form model [14].

More recently, studies have indicated that blood flow is the decisive factor in AAA. Phan et

al. [15] modelled aneurysms taking into account both the blood flow and the physical properties of the tissues. Ene et al. [16] compared the results obtained only with numerical simulation of fluid flow by Computational Fluid Dynamic (CFD) with those from Fluid-Solid Interaction (FSI) simulations. These authors reported values that were approximately 5% higher in terms of both strains and Von Mises stresses in the FSI model. The difference in shear stress is 35% at the level of the wall. To summarize, in order to better model AAA, determining the stresses in the wall of an aneurysm requires accurate measurement its geometry and deformation, as well as measurement of the hemodynamic flow.

To evaluate AAA, medical teams commonly use ultrasound, Computed Tomography (CT scanner), Magnetic Resonance Imaging (MRI), ray radiography or intravascular Doppler imaging. Few studies are based on experiments that measure stresses using, e.g., photoelasticity [17,18] or deformations via ultrasound [19]. Similarly, few studies have experimentally measured blood velocities. Salsac et al. [20] performed flow measurements by Particle Image Velocimetry (PIV) and showed the turbulence created in the aneurysm. In a work by Deplano et al. [21], experiments were conducted on rigid asymmetric AAA models using glass and deformable polyurethane under conditions of rest and exercise.

In the present study, Magnetic Resonance Imaging (MRI) is considered because it provides a detailed anatomical analysis thanks to tomographic slices according to any orientation and within radiation (such as CT scan). MRI can thus measure not only physical characteristics but also blood flow. Although CT-scan imaging is recognized as the gold standard to study anatomy of the aorta, among all cardiovascular imaging techniques, by providing high contrast among the structures and kinetic images, MRI is well suited to dynamically evaluate AAA. Recent approaches in 4D flow study with MRI have enabled a better understanding of the flow in the aorta.

The settings of the MRI devices and the measurement protocol must be adapted to each type of measurement. However, there is not always certainty about the reliability and accuracy of the measuring data. It is therefore necessary to validate the results obtained by comparing them with those obtained by other suitable techniques. The present study follows-up an initial analysis of the use of MRI to measure strains [22]. In this study, experiments are performed to measure local blood flow velocities. The experimental results are obtained using 2D +time MRI, 4D flow MRI and PIV.

In a first portion of the study, the measuring protocol for each technology is presented for the analysis of a pulsed flow in a cylindrical glass phantom in as close to physiological conditions as possible. Then, in a second step, the measurements of a complex flow on a deformable silicone phantom with an axisymmetric aneurysm are compared and discussed.

Method and Materials

Experimental procedure: *in vitro* tests

A device to reproduce a pulsatile flow in a phantom was developed without magnetic material, as required by the constraints of MRI measurements. This device, shown in (Figure 1), is removable and transportable because the used MRI and PIV facilities are located at different locations. The device establishes a pulsed flow through a piston pump with a period of 0.8s and transmits this flow through pipes to the test device, where the phantom is attached. This chamber allows immersion of the phantom in a liquid (water) to (i) view its external wall in MRI and (ii) overcome the refractive problems due to the wetting surface of silicone in PIV. Pressure sensors and a flow meter allow controlling the characteristics of the flow, which is regulated by two valves. For all of the tests, the mean flow rate was constant and equal to 4l/min. The pressure varied between 0 and 250mbar depending on the pump cycle, providing greater values of systolic pressure and lower value of diastolic pressure. In this experiment, the conditions are not necessarily identical to physiological conditions within a patient. Water as the flow agent as chosen despite its lower viscosity than that of blood. This choice not

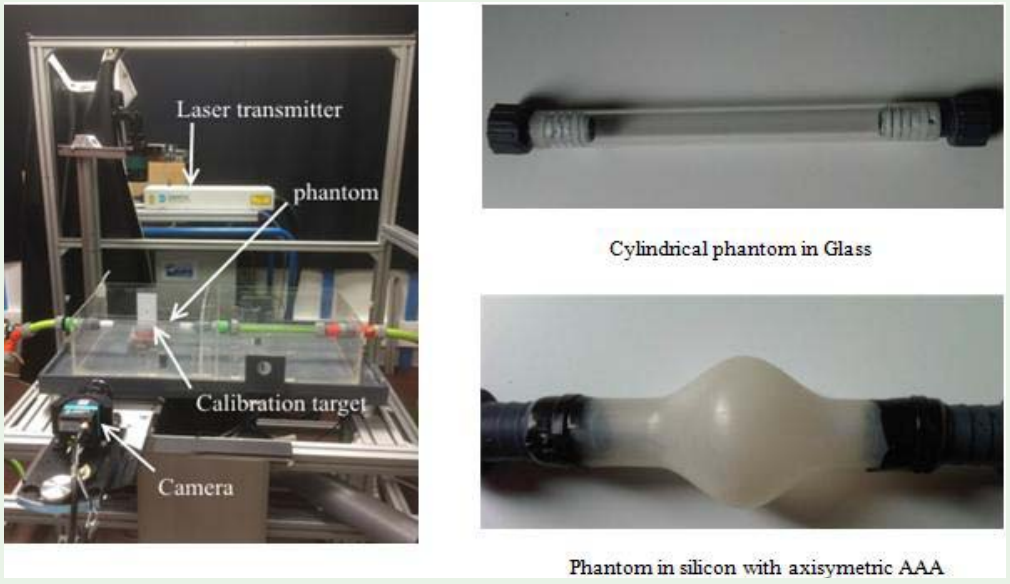

Figure 1: Experimental device in its configuration for PIV (left) glass phantom and axisymmetric phantom of AAA in silicone (right).

Citation: Wang Y, Joannic D, Juillion P, Kemrones A, Monnet A, Lalande A, et al. Comparison of Flow Measurement by 4D Flow Magnetic Resonance Imaging and by Particles Image Velocimetry on Phantom of Abdominal Aortic Aneurysm. SM Vasc Med. 2016; 1(2): 1008.

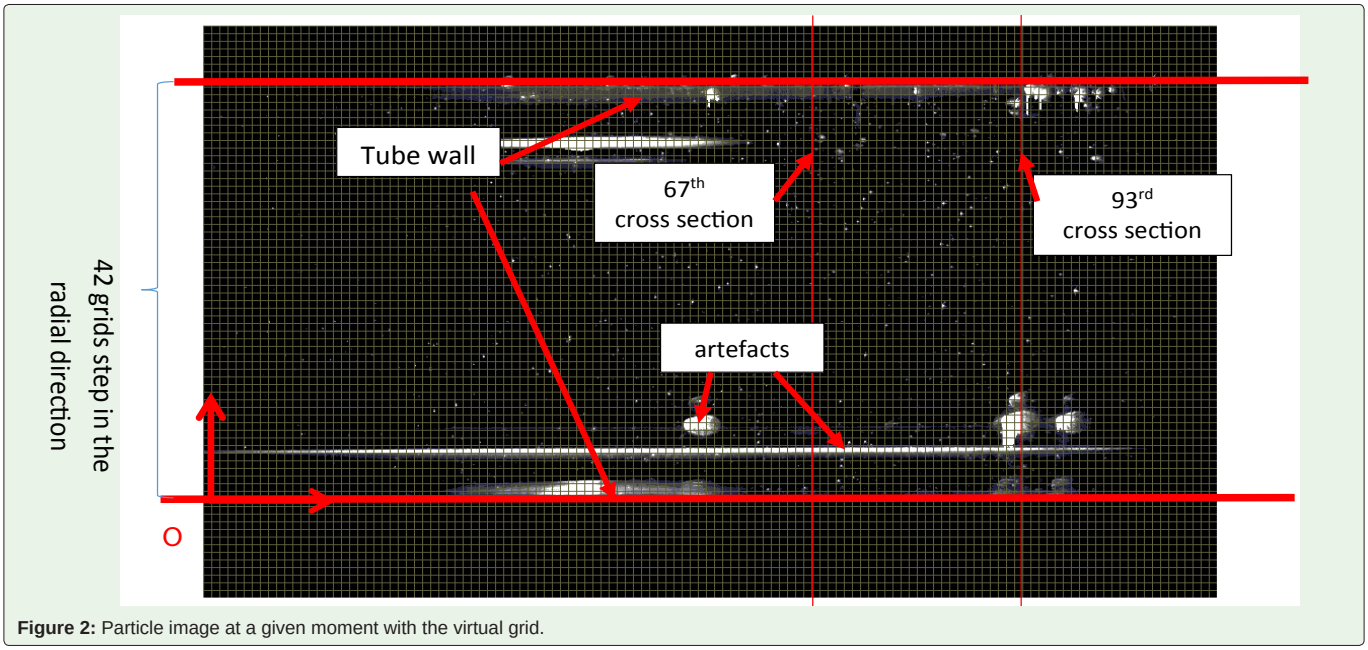

Figure 2: Particle image at a given moment with the virtual grid.

only allows more flexibility for dosing and cleaning than the usual mixture of water and glycerin but also allows temperature control because the viscosity of glycerin is strongly temperature dependent.

A first test consists of performing comparative measurements of a pulsating flow in an undeformable phantom in glass. The generated velocity field is relatively simple and has variable axial components according to the radius and over time. One of the advantages of this phase is that it has an analytical based on the Womersley model and allows validation of the results. This solution is given by the following equation (1):

$$V(r,\omega,t) = -j\frac{\Delta p_0}{\rho L\omega}e^{j\omega t}\left(\frac{1-J_0\left(\alpha\sqrt{-j}\right)}{1-J_0\left(\alpha_0\sqrt{-j}\right)}\right) \quad (1)$$

With $\alpha = r\sqrt{\frac{\rho\omega}{\mu}}$ and $\alpha_0 = r_0\sqrt{\frac{\rho\omega}{\mu}}$,

where r is current radius, r_0 is interior radius of the cylinder, ω is the pulsation, J_0 is the 0-order of Bessel's function, ρ is the density, ΔP_0 is the differential pressure and μ is the dynamic viscosity.

In these flow conditions, an in plane velocity mapping MRI is used because the flow is simple and the cross section planes are sufficient to determine the velocity flow. In parallel, PIV is carried out in a single plane containing the axis of the tube.

A second more realistic test makes use of on a deformable phantom in silicone with an axisymmetric fusi form aneurysm. This phantom simply but effectively reproduces the flow behavior of a real AAA.

If the flow is axisymmetric, 4D flow MRI sequence were used because several 2D sequences according to different orientations are needed to reconstruct its characteristics. For PIV, as in the previous case, a single plane containing the axis of the phantom is obtained.

Flow measurement by PIV

Cylindrical glass phantom: PIV is an imaging technique that can measure instantaneous speed fields by acquiring images of particles over a very short time period. A Dantec® machine was used in this study. Fluorescent particles of Rhodamine (20 μmin diameter) were introduced into the water and set in motion via the experimental arrangement (Figure 1). The measurement rate was 12 frames per cycles. It is common that 200 replicates are required to perform transient measurements due to the spatial dispersion of the particles. In this way, by averaging, a representative response of the velocities over the whole of the field can be obtained. Thus, for each test, 2400 images of an axial section of the field were considered, acquired and processed.

The variability of PIV measurements on a complete cycle was quantified to define theme trological performance of the system. To this end, pulsed flow tests were conducted on a cylindrical phantom in glass, with a pressure level ranging from -60 to 173 mbar.

The objective of these tests was (i) to assess the dispersions due to the location of the measurement field (at each moment, the flux considered is constant for all of the cross sections along the axis of the phantom) and (ii) to provide a basis of comparison for the measurements obtained in the same conditions as in the MRI.

To process the images acquired by PIV, image correlation software was used. The region of interest (ROI) was composed of 123 square mesh elements (5 x 5 pixels each) in the axial direction and 42 elements in the radial direction. Note that in the image in (Figure 2) artifacts are created by parasitic reflections on the wall. It is therefore necessary to choose the most feasible study area that is free of these reflections.

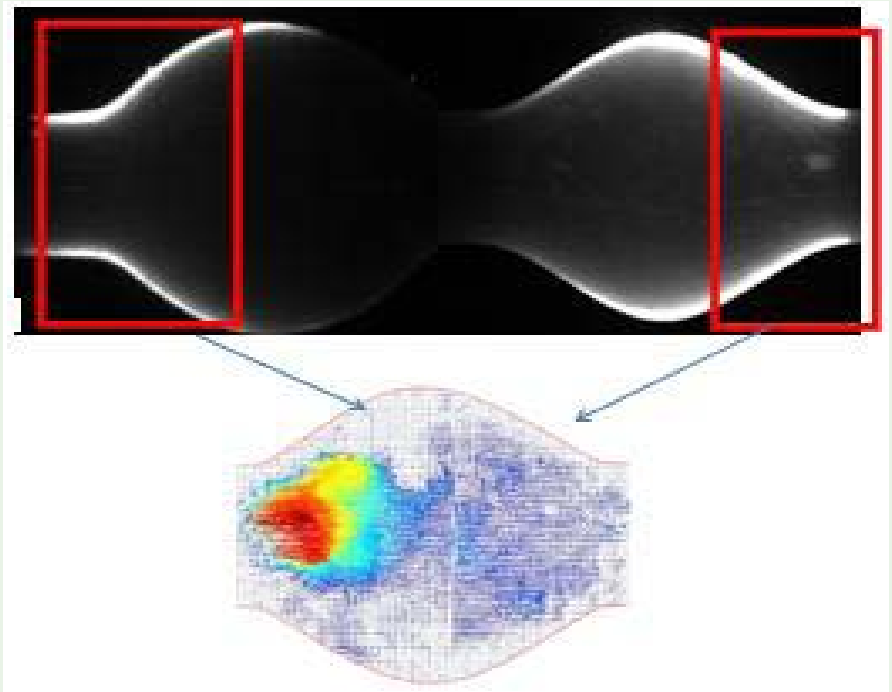

Figure 3: Reconstruction of the region of interest by matching the both images for each proximal and distal region of the aneurysm.

The PIV results were analysed and compared for several sections. A small amount of noise is observed due to the influence of reflections on the patterns correlation, the absence of particles on a grid element or instability caused by flow pulsation. However, results differences are weak, validating the measurement quality.

The operating conditions were similar to those of the cylindrical sample in glass. However, the camera's field of view does not completely cover the proximal and distal regions of the phantom. Two positions of the camera were required, and the connection of the two areas was carried out by matching, as shown in (Figure 3).

Flow measurement by MRI

To evaluate the vector field representing the instantaneous flow from MR data, a 4D velocity mapping sequence was used. 4D flow MRI offers the ability to measure and visualize the temporal evolution of complex blood flow patterns within an acquired 3D volume [23]. To summarize the principle of the acquisition sequence, the flow velocity information can be encoded according to the changes in the MR signal phase along a magnetic field gradient. Using appropriate bipolar velocity encoding gradients (one for each space direction), flow-dependent phase changes can be detected by performing two acquisitions with different velocity-dependent signal phases [23]. Subtraction of the resulting phase images allows the quantitative assessment of the velocities of the underlying flow or motion [24]. The user must define the upper velocity limit (Venc), and this value defines the maximum velocity (positive or negative, according to the direction) that can be encoded without aliasing artifacts. When defining the settings of the sequence, the maximum velocity must be slightly higher than the expected maximum speed whatever the direction. Stationary material return a mid-grey colour (i.e., zero-value pixels), and increasing velocities in opposite directions are shown as brighter (positive pixels) or darker (negative pixels), with the shade exhibiting an accurate linear relationship to velocity [25]. Velocity-encoded images are usually acquired on human studies with ECG-gated techniques with respiratory gating. For each moment of the cardiac cycle, a magnitude image (corresponding to an anatomic image) and a phase image depicting the flow are created. In our study, 4D flow MRI measurements were taken on a 3 Tesla magnetic whole body imager (Trio TIM, Siemens Medical Solutions, Germany) using a phased-array thoracic coil centered on the phantom. Water container with diluted gadolinium-based contrast agent was used to simulate blood inside the phantom. The measurements were performed without respiratory gating and were prospectively gated with the pressure signal given by the pressure sensor. The imaging parameters were as follows: velocity encoding (Venc) = 160cm/sec in all 3 directions; TE = 2.83; TR = 5.7; rectangular FOV = 256 × 128 mm^2, slab thickness = 3 mm, including the entire phantom; spatial resolution = 0.78 × 0.78 × 3 mm^3. The total acquisition time was of the order of 20 minutes, with a temporal resolution for each 3D time frame of 27.5 msec.

Data were post-processed with the Siemens 4Dflow software. Among the 4D volume of data, we can select a specific slice with an orientation perpendicular to main axis of the phantom. On this slice, the area surface of the phantom can be determined from anatomic images, and a region of interest (ROI) corresponding to this surface was defined for each image. The mean velocity for each phase was calculated on each corresponding phase image by applying the same ROI as that defined on the magnitude images (the velocity can also be calculated for each pixel of this ROI). The curve representing the evolution of the velocity against time was then constructed. Moreover, the instantaneous flow was determined by considering the velocity and the surface of the ROI. By considering these data over the whole cycle, the total flow was calculated.

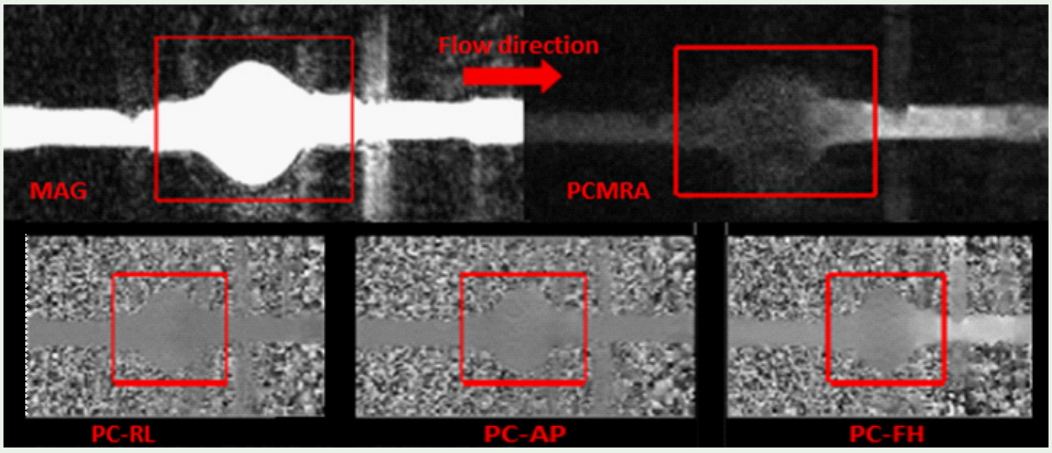

Figure 4: Examples of images acquired by 4D flows MRI for an axisymmetric AAA phantom.

Figure 4 shows the images acquisition by 4D flow MRI for the axisymmetric AAA phantom. Top left, the images was acquired in magnitude (MAG). Top right they were made using Phase Contrast Magnetic Resonance Angiography (PCMRA). These images allow visualization of the overall blood flow in the vessels using flow-sensitive MRI. The last three images are taken from three different orientations and coding (RL-Right to left; AP-Anterior to posterior; FH (Foot-to-head) for Phase Contrast Image (PC).

Results

Validation of the device with the cylindrical glass tube

The velocity profiles of the measurements made using the MRI and PIV and calculations with the Wormesley model were compared at the level of the 93rd section determined on the PIV (see Figure 2).

Figure 5 shows the comparison for 12 time points within the cycle. Good concordance can be observed between the curves for high velocities. In contrast, there is a slight gap between the curves for velocities close to zero. Indeed, as for all MR imaging techniques, 4D flow MRI is slightly noisy, which can lead to errors in the determined velocities; in addition, an uncorrected offset can appear for low velocity values. For various reasons (e.g, uncorrected Maxwell equations, eddy currents, small gradient waveform errors, and random noise), all tissues can show small errors in velocity measurements. These errors may be uniform or can vary (linearly or non-linearly) across the image [25]. These errors involve phase deviations and result in differences between the velocity calculated by MRI and PIV for low-velocity measurements. Considering the whole ROI, the maximum average speed is equal to 0.45 m/s with the MR data and 0.48 m/s for the PIV determination, corresponding to an error of 6.25 %.

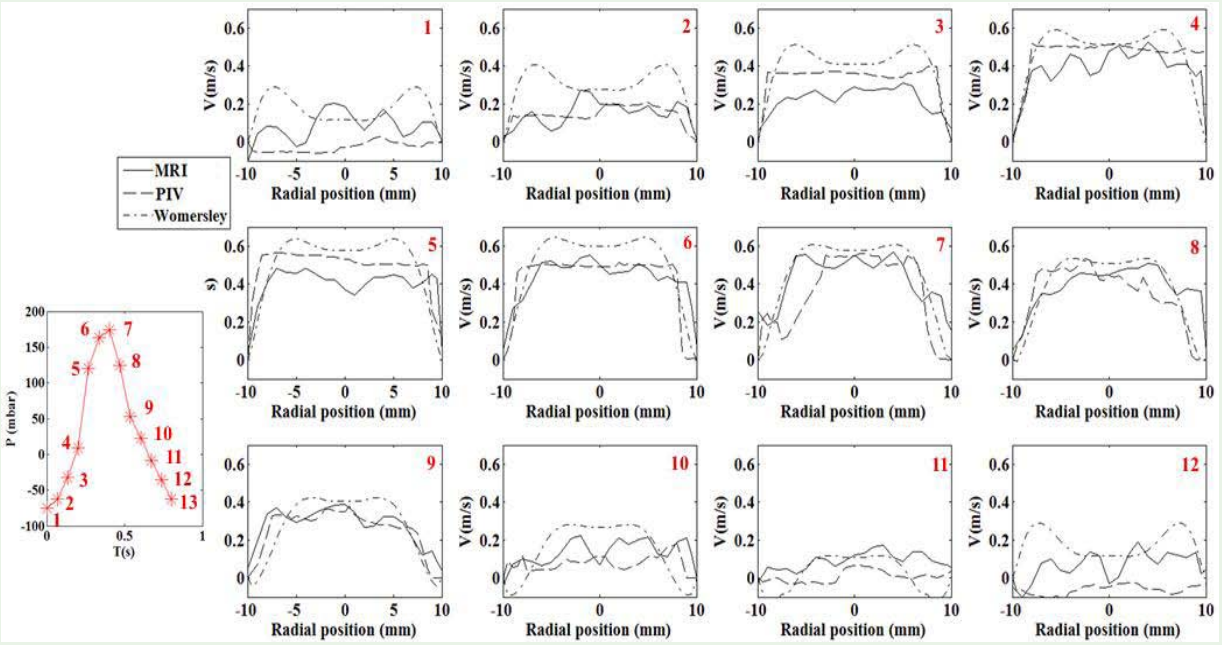

Figure 5: Comparison of experimental results (MRI and PIV measurements) with theoretical results (Wormesley's model) at different pressures of simulated cardiac cycle.

Citation: Wang Y, Joannic D, Juillion P, Kemrones A, Monnet A, Lalande A, et al. Comparison of Flow Measurement by 4D Flow Magnetic Resonance Imaging and by Particles Image Velocimetry on Phantom of Abdominal Aortic Aneurysm. SM Vasc Med. 2016; 1(2): 1008.

Table 1: Comparison of the average flow rates obtained by PIV, MRI and the flow meter for one simulated cardiac cycle.

	Mean Velocity on a cross section at t=0.4s	Flow rate (L/min)	Relative error at flow meter
PIV	0.48 m/s	4.088	2.5%
MRI	0.45 m/s	4.166	4.6%
Flow meter	×	3.98	×

The flow rate over a cycle is given in (Table 1). A good fit with the value given by the flow meter is obtained.

Results of PIV and MRI measurement for phantom in silicon with axisymmetric AAA

PIV results: Figure 6 shows the velocities determined at different times within the cycle. Errors are present at the junction the images due to (i) the poor detection of particles at the limit of the field of view and (ii) the effects of image reconstruction. Flow is primarily observed within the central area of the phantom, and little flow is observed within the aneurysmal sac. However, it is difficult to draw conclusions from these data. Indeed, it is difficult to make quality measurements near the phantom wall because of the refraction of the laser plane through the wall's thickness.

MRI results: Figure 7 shows the flow for different time points during the cycle. The first 9 images show the arrival of the pulsatile flow (t = 0 to 0.4s), and the last three show the phase corresponding to a virtual steady state after the passage of the flow wave (t = 0.4 to 0.8s). The flow is clearly visible and is primarily concentrated in the central portion of the aneurysm. There is a slight vortex within the aneurysmal sac. Unlike the PIV experiment, this vortex is clearly observable.

Discussion

A qualitative comparison can be made between PIV and MRI with respect to the measurement of velocity fields in the AAA phantom during a simulated cardiac cycle. The primary conclusions are as follows:

-the fluid velocity is always higher at the centre of the AAA phantom, and fluid velocity is very low within the aneurysmal sac (see Figures 6 and 7).

-at approximately 0.12 s into the cycle, a very small vortex begins to form due to the sudden arrival of flow. The phantom then grows as fluid velocity increases. The vortex expands until it completely occupies the sac. Between t=0.37s and t=0.44s, the elasticity of the wall acts on the flow. The wall then returns to its original state by pushing the flow of the sac toward the middle of the phantom. From0.5 s onward, the flow is close to zero until the next pulse.

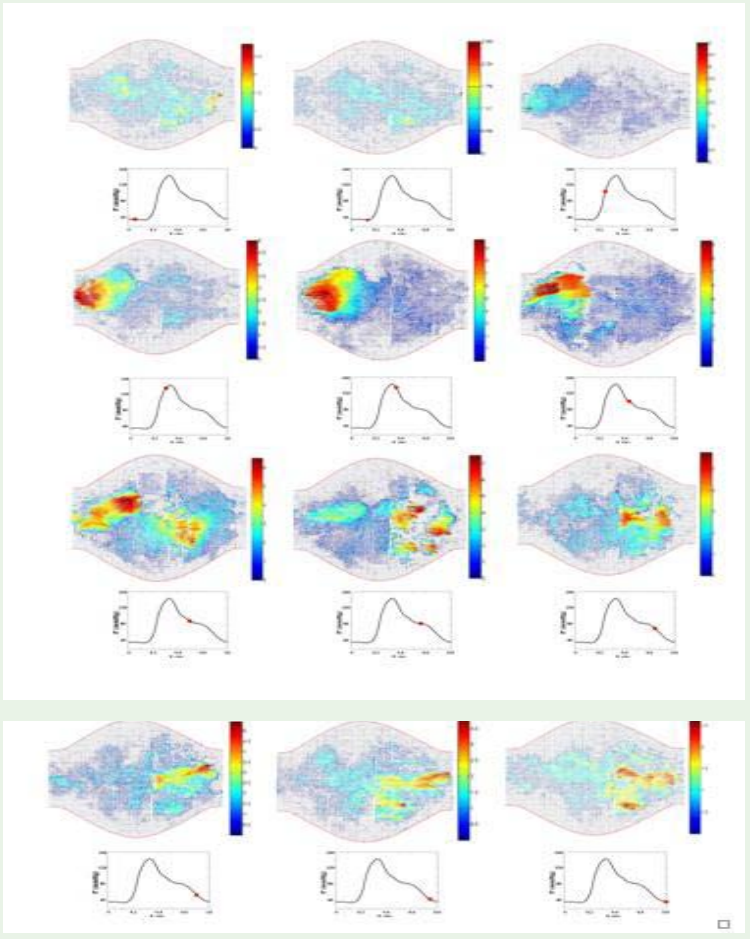

Figure 6: Cartography of velocities, measured by PIV, of a axisymmetric AAA phantom in silicone (time t=0 corresponds to the maximum pressure at inlet level).

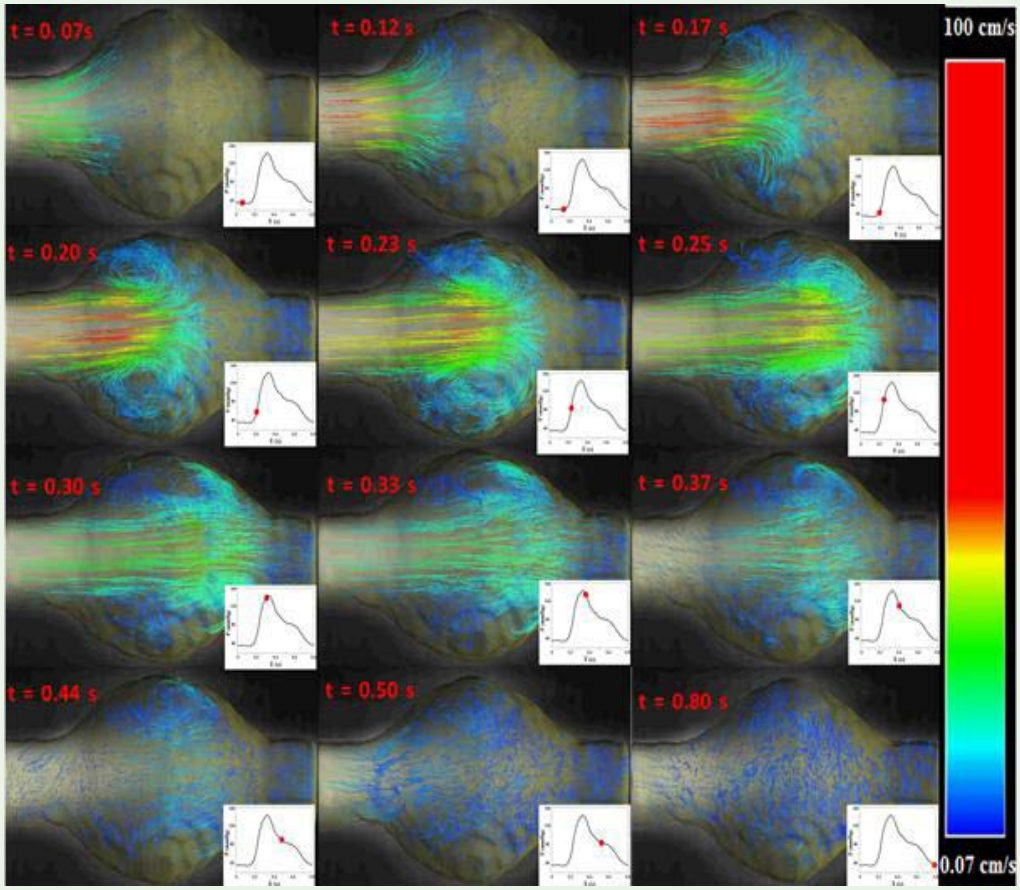

Figure 7: Evolution of velocities fields measured by 4D flows MRI for the case of an axisymmetric AAA phantom in silicone.

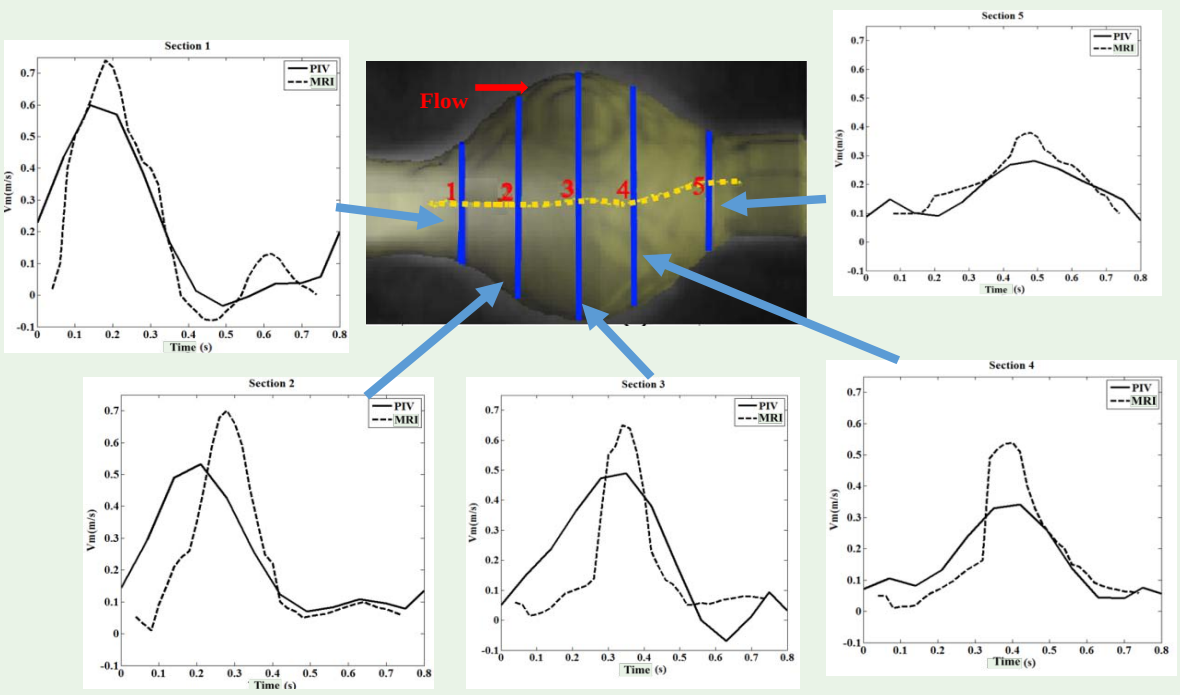

Figure 8: Evolution of the average velocity in cross sections during the cycle determined by MRI and PIV.

Citation: Wang Y, Joannic D, Juillion P, Kemrones A, Monnet A, Lalande A, et al. Comparison of Flow Measurement by 4D Flow Magnetic Resonance Imaging and by Particles Image Velocimetry on Phantom of Abdominal Aortic Aneurysm. SM Vasc Med. 2016; 1(2): 1008.

This first qualitative comparison allows us to better understand the velocity field and its evolution, especially within the aneurysmal sac. This result confirms that it is possible to measure velocity fields by 4D flow MRI. The velocity field remains too complex to make a direct quantitative comparison with PIV. The flow is primarily located in the centre of the phantom, and comparison of the average flow speed evolution within central sections of the phantom over the cycle gives interesting results (see Figure 8). The cross sections are positioned similarly for both measurement methods, and their areas are nearly identical, with a maximum deviation of 3%. As the PIV measurements were carried out only along a single plane, the reported velocity values are based on the assumption of a velocity field with a quasi-axial symmetry. The PIV vs. MRI comparison is performed only for the component of velocity in the axial direction of the phantom. Figure 8 shows the evolution of the average velocity for both methods.

It should be noted that, in both measurement techniques, an initial tendency for decreased flow was observed. This effect is due to the geometry of the phantom, which disperses the flow within the sac. It is notable that the flow wave as measured by MRI was always approximately 30% higher than the PIV measurements. This discrepancy may be caused by measurement uncertainty with PIV (e.g., missing data; reconstruction, notably for section 3). Additional acquisitions are needed to render the PIV more reliable. It was not possible in this study to show the influence of the deformation of the wall. Indeed, a glass phantom has been developed but the operating conditions have not been sufficiently satisfactory to make objective comparisons between rigid and deformable walls. However, several limitations lie in this study compared to the *in vivo* conditions.

First, the fluid used (water) has a lower viscosity than the blood. This difference does not however constitute a disadvantage in the sense that the lower the viscosity, the more pronounced the turbulences of the fluid. The ability of MRI to measure flows is therefore more critical in this case, so the MRI measurement of blood flow will be more accurate.

Finally, an AAA often presents a thrombus. In this case, the flow is of course perturbed and the thrombus tends to stiffen the wall. Works in progress take into account the non-symmetry of the AAA from measurements obtained on a realistic phantom developed on the basis of measurements taken on a patient.

Conclusion and Perspectives

In conclusion, this comparison shows that 4D MRI and PIV provide consistent flow measurement results. The results obtained using these two techniques also generally shows a certain degree of consistency with respect to the determination of velocities fields. For a simple pulsed field, the two technologies provide similar results that correlate well with the theory. For more complex fields of phantom with aneurysms, the velocity fields are difficult to compare directly because of measurement noise; however, the measurements by 4D flow MRI correlate quite well with those made by PIV. The 4D MRI flow measurement technique can therefore be used to reliably diagnosis AAA. Tests on realistic phantoms are underway and the results are promising.

Acknowledgement

M. Mathieu of Danielson society, Magny-Court, France, for his help for the PIV measurements.

This study received financial assistance from the Burgundy Regional Council through the European fund.

References

1. Raghavan M L, Vorp D A. Toward a biomechanical tool to evaluate rupture potential of abdominal aortic aneurysm: identification of a finite strain constitutive model and evaluation of its applicability. Journal of Biomechanics. 2000; 33: 475-482.
2. Di Achille P, Celi S, Di Puccio F, Forte P. Anisotropic AAA. Computational comparison between four and two fiber family material models. J Biomech. 2011; 44: 2418-2426.
3. Truijers M, Pol JA, SchultzeKool LJ, van Sterkenburg SM, Fillinger MF, Blankensteijn JD. Wall stress analysis in small asymptomatic, symptomatic and ruptured abdominal aortic aneurysms. European Journal of Vascular and Endovascular Surgery. 2007; 33: 401-407.
4. Rodriguez J F, Ruiz C, Doblare M. and Holzapfel G.A. Mechanical stresses in abdominal aortic aneurysm. Material anisotropy a parametric study. Onate and D R J. Owen, editors. In: CIMNE. 2007; 248-252.
5. Reeps C, Gee M, Maier A, Gurdan M, Eckstein H H, Wall W. A. The impact of model assumptions on results of computational mechanics in abdominal aortic aneurysm. Journal of Vascular Surgery. 2010; 51: 679-688.
6. Choudhury N, Bouchot O, Rouleau R, Tremblay D, Cartier R, Butany J, et al. Local mechanical and structural properties of healthy and diseased human ascending aorta tissue. Cardiovascular Pathology. 2009; 18: 83-91.
7. Iliopoulos D C, Deveja R P, Kritharis E P, Perrea D, Sionis G D, Toutouzas K, et al. Regional and directional variations in the mechanical properties of ascending thoracic aortic aneurysms. Medical Engineering & Physics. 2009; 31: 1-9.
8. Duprey A, Khanafer K, Schlicht M, Avril S, Williams D, Berguer R, et al. In Vitro Characterisation of Physiological and Maximum Elastic Modulus of Ascending Thoracic Aortic Aneurysms Using Uniaxial Tensile Testing. European Journal of Vascular and Endovascular Surgery. 2010; 39: 700-707.
9. Karimi A, Navidbakhsh M, Shojaei A, Faghihi S. Measurement of the uniaxial mechanical properties of healthy and atherosclerotic human coronary arteries. Materials Science and Engineering C, Materials for Biological Applications. 2013; 33: 2550-2554.
10. Tong J, Cohnert T, Regitnig P, Holzapfel G A. Effects of age on the elastic properties of the intraluminal thrombus and the thrombus-covered wall in abdominal aortic aneurysms: biaxial extension behavior and material modeling. European Journal of Vascular and Endovascular Surgery. 2011; 42: 207-219.
11. Avril S, Badel P, Duprey A. Anisotropic and hyperelastic identification of in vitro human arteries from full-field optical measurements. J Biomech. 2010; 43: 2978-2985.
12. Toungara M, Geindreau C. Fluid structure interaction and material model influence on stresses distribution in abdominal aortic aneurysms. In: 9th international Symposium on Computer Methods in Biomechanics and Biomedical Engineering. 2010; 24-27.
13. Scotti CM, Finol EA. Compliant biomechanics of abdominal aortic aneurysms: A fluid-structure interaction study. Computers & Structures. 2007; 85: 1097-1113.
14. Wang DH, Makaroun MS, Webster MW, Vorp DA. Effect of intraluminal thrombus on wall stress in patient-specific models of abdominal aortic aneurysm. J Vasc Surg. 2002; 36: 598-604.
15. Pham T, Martin C, Elefteriades J, Sun W. Biomechanical characterization of ascending aortic aneurysm with concomitant bicuspid aortic valve and bovine aortic arch. Acta Biomater. 2013; 9: 7927-7936.
16. Ene F, Gachon C, Delassus P, Carroll R, Stefanov F, O'Flynn P, Morris L. In vitro evaluation of the effects of intraluminal thrombus on abdominal aortic aneurysm wall dynamics. Medical Engineering & Physics. 2011; 33: 957-966.

17. Morris L, O'Donnell P, Delassus P, Mc Gloughlin T. Experimental Assessment of Stress Patterns in Abdominal Aortic Aneurysms using the Photoelastic Method. Strain. 2004; 40: 165-172.

18. Doyle BJ, Killion J, Callanan A. Use of the photoelastic method and finite element analysis in the assessment of wall strain in abdominal aortic aneurysm models. Journal of Biomechanics. 2012; 45: 1759-1768.

19. Bihari P, Shelke A, New TH, Mularczyk M, Nelson K, Schmandra T, Knez P, Schmitz-Rixen T. Strain Measurement of Abdominal Aortic Aneurysm with Real-time 3D Ultrasound Speckle Tracking. European Journal of Vascular and Endovascular Surgery. 2013; 45: 315-323.

20. Salsac AV, Sparks SR, Chomaz JM, Lasheras JC. Evolution of the wall shear stresses during the progressive enlargement of symmetric abdominal aortic aneurysms. J of Fluid Mechanic. 2006; 560: 19-51.

21. Deplano V, Meyer C, Guivier-Curien C, Bertrand E. New insights into the understanding of flow dynamics in an in-vitro model for abdominal aortic aneurysms. Medical Engineering & Physics. 2013; 35: 800-809.

22. Wang Y, Joannic D, Delassus P, Lalande A, Juillion P, Fontaine J.F. Comparison of the strain field of abdominal aortic aneurysm measured by MRI and stereovision: A feasibility study for prediction of the risk of rupture of AAA. Journal of Biomechanics. 2015; 48: 1158-1164.

23. Mark M, Frydrychowicz A, Kozerke S, Hope M, Wieben O. 4D flow MRI. J Magn Reson Imaging. 2012; 36: 1015-1036.

24. Pelc NJ, Bernstein MA, Shimakawa A, Glover G.H. Encoding strategies for three-direction phase-contrast MR imaging of the flow. Journal of Magnetic Resonance Imaging. 1991; 1: 405-413.

25. Gatehouse PD, Keegan J, Crowe LA, Masood S, Mohiaddin RH, Kreitner KF, et al. Applications of phase-contrast flow and velocity imaging in cardiovascular MRI. Eur Radiol. 2005; 15: 2172-2184.